

# Polarized angular dependent spectroscopy of epithelial cells and epithelial cell nuclei to determine the size scale of scattering structures

J. R. Mourant  
T. M. Johnson  
S. Carpenter  
A. Guerra  
T. Aida  
J. P. Freyer

Los Alamos National Laboratory  
Bioscience Division  
Los Alamos, New Mexico 87545

**Abstract.** An understanding of the relationship between tissue structures and light scattering from tissue will help facilitate the development and acceptance of noninvasive optical diagnostics including elastic scattering spectroscopy, diffuse reflectance, and optical coherence tomography. For example, a quantitative model of the structures that scatter light in epithelial cells would allow determination of what structures control the characteristics of *in vivo* light transport measurements and subsequently could provide a detailed relationship between cellular structures and optical measurements. We have determined the size distribution of refractive index structure variations in epithelial cells as well as in nuclei isolated from epithelial cells from measurements of the angular dependence of polarized light scattering. The quantitative size distributions we obtained for both whole cells and isolated nuclei include particles with effective radii of 2  $\mu\text{m}$  to 10 nm or less and contain orders of magnitude more small particles than large particles. These results demonstrate that not only are biological cells very heterogeneous, but so are the nuclei within them. Light scattering is likely sensitive to structures smaller than those commonly investigated by standard pathology methods. © 2002 Society of Optical Instrumentation Engineers. [DOI: 10.1117/1.1483317]

Paper TP-09 received Sep. 27, 2001; revised manuscript received Feb. 7, 2002; accepted for publication Mar. 11, 2002.

## 1 Introduction

The scattering of linearly polarized light from index-of-refraction variations is quite sensitive to the size and shape of the index variations as well as to the actual magnitude of the refractive-index changes. Consequently, polarized light scattering is being investigated as a possible noninvasive tissue diagnostic by several research groups. In a backscattering geometry, images of a turbid media such as tissue, viewed through a polarizer either parallel or crossed to the incident polarization, have several prominent characteristics that depend on the morphology of the scattering centers in the object being imaged.<sup>1,2</sup> The dependencies of image features on spherical particle size and on particle concentration have been well studied and can be modeled using Monte Carlo propagation of polarized light through tissue.<sup>3–6</sup> The wavelength dependence of polarized, backscattered light has also been shown to be very sensitive to the size of spherical particles.<sup>7</sup> Backman et al.<sup>8</sup> and Sokolov et al.<sup>9</sup> have analyzed the wavelength dependence of the backscattering of polarized light to infer information about the size and/or refractive index of nuclei in epithelial cells. Backman et al.<sup>8</sup> subtracted the directly backscattered light polarized perpendicular to the incident polarization from the directly backscattered light polarized parallel to the incident polarization. The wavelength dependence of this intensity was then fit to a Mie theory model that assumed single backscattering from a distribution of spherical scatterers. The fit presented in the paper gave a

size distribution of sphere sizes that agreed quite well with microscopic measurements of nuclear size. Sokolov et al.<sup>9</sup> measured the depolarization ratio,  $(I_{\parallel} - I_{\perp}) / (I_{\parallel} + I_{\perp})$ , of the backscattered light from cervical biopsies. The resulting wavelength dependent curve was then fit to a sum of forward ( $-5^{\circ} - 5^{\circ}$ ) and backward ( $139^{\circ} - 149^{\circ}$ ) Mie scattering, and a dc offset. The forward and backward components were both calculated from two size distributions of spherical scatterers with fixed widths. The smaller of the two means of the size distributions was assumed to represent scattering from the nucleus while the larger was assumed to be represent scattering from the whole cell. The obtained value of 8  $\mu\text{m}$  for the diameter of the nucleus was slightly bigger than the value of 6.1  $\mu\text{m}$  the authors cite from morphometric measurements. Finally, with the goal of developing *in vivo* techniques, our group has developed a fiberoptic probe for measuring the propagation of polarized light through tissue.<sup>10</sup> Measurements with this probe can be used to obtain information about both the effective particle size and the concentration of polystyrene sphere suspensions.

In addition to the work mentioned above to understand the backscattering of polarized light from a turbid media composed of spheres, several research groups have looked into the fundamentals of polarized light transmission through a turbid media. The rate at which linearly polarized light is depolarized depends on both the ratio of the refractive index of the scatterer,  $n_s$ , to the medium refractive index,  $n_m$ , and on the particle size parameter,  $2\pi r n_m / \lambda$ , where  $r$  is radius and  $\lambda$  is

Address all correspondence to Judith Mourant. Tel: 505-665-1190; Fax: 505-665-4637; E-mail: jmourant@lanl.gov

wavelength. For a given scattering coefficient and wavelength, depolarization occurs over a shorter distance for spheres with a smaller size parameter.<sup>11–13</sup>

In order for polarized light scattering to reach its potential as a tool for noninvasively probing tissue and cellular architecture, a fundamental understanding of the structural features that scatter light in biological materials is needed to enable a detailed understanding of polarized light propagation in tissue. Tissues and biological cells are composed of biochemical materials with a variety of refractive indices. Additionally, there are a wide variety of structures within mammalian cells. Nuclei are on the order of 5–10  $\mu\text{m}$  in diameter,<sup>14</sup> mitochondria, lysosomes and peroxisomes have dimensions on the order of 1–2  $\mu\text{m}$ , ribosomes are on the order of 20 nm in diameter<sup>15</sup> and structures within various organelles can have dimensions up to a few hundred nanometers. Schmitt and Kumar demonstrated that the spectrum of index variations exhibits power-law behavior for a wide range of spatial frequencies.<sup>16</sup> Consequently, biological cells have been hypothesized to scatter light as if they were composed of particles with a wide range of sizes and a model with a broad range of discrete particle sizes has been proposed.<sup>17</sup>

One goal of the research described in this paper was to use the acute sensitivity of polarized light scattering to refractive index structure in order to refine and test quantitative models for the size and shape of scattering centers in epithelial cells. A second goal was to determine the length scale of the refractive index variations in epithelial nuclei.

## 2 Methods

### 2.1 Cell Lines and Culture

AT3.1 and AT6.1 are androgen-independent malignant rat prostate carcinoma cells<sup>18</sup> kindly supplied by Dr. Rinker-Schaeffer of the University of Chicago. Cells were cultured in  $\alpha$ -MEM (Invitrogen) containing 10% (V:V) fortified calf serum (Hyclone Laboratories) and antibiotics (50  $\mu\text{g}/\text{mL}$  streptomycin and 50 U/mL penicillin, Invitrogen) referred to hereafter as complete medium. Monolayer cultures were maintained in treated polystyrene culture flasks or dishes in a 37 °C incubator containing a humidified atmosphere of 5% CO<sub>2</sub> and 95% air. Cells were detached from dishes by incubation in 0.25% trypsin (DIFCO) in Puck's saline A containing 1 mM EDTA and 25 mM N-[2-hydroxyethyl]piperazine-N'-[2-ethanesulfonic acid] (HEPES) (Sigma Chemicals) at pH 7.4. After the addition of complete medium, cell suspensions were passed twice through an 18-gauge needle to disrupt cell clumps. For light scattering measurement, cell suspensions were centrifuged (1500 rpm for 10 min) then resuspended in ice-cold phosphate-buffered saline (PBS) (Invitrogen) and stored on ice until analysis. Counts performed after light scatter analysis showed no significant loss of cells after several hours of storage in PBS on ice.

### 2.2 Cell Counting and Volume Analysis

Three counts of each cell suspension were determined with an electronic particle counter (Coulter Electronics) interfaced to a pulse-height analyzer. Counts were only taken on that region of the cell volume distribution that excluded small-volume acellular debris. A cell volume distribution containing  $>10^4$  cell measurements was saved for each sample and analyzed to

estimate the mean cell volume of the population. Volumes were calibrated by measurement of polystyrene spheres 7–21  $\mu\text{m}$  in diameter.

### 2.3 Nuclei Isolation and Measurement

Nuclei were isolated from cells using a selective cell lysis and gradient centrifugation procedure as follows. Cells were centrifuged and resuspended at a concentration of  $6\text{--}8 \times 10^6$  cells per mL in a hypotonic lysis buffer (HLB: 5 mM KCl, 1.5 mM MgCl<sub>2</sub>, 10 mM tris[hydroxymethyl]-aminomethane (TRIS, Sigma Chemicals) at pH 7.9) and incubated for 10 min on ice. This suspension was then passed six times through a 22-gauge needle to lyse the cells and release intact nuclei. The nuclear suspension was then layered on top of a sucrose cushion (800 mM sucrose in HLB) and centrifuged at 6000 rpm for 10 min. The resulting pellet was resuspended in a sucrose buffer (250 mM sucrose, 3.3 mM MgCl<sub>2</sub>, 10 mM TRIS at pH 7.9) then centrifuged (1000 rpm for 5 min) and resuspended in sucrose buffer (250 mM sucrose, 10 mM MgCl<sub>2</sub>). This suspension was then layered on top of a second sucrose cushion (250 mM sucrose, 0.5 mM MgCl<sub>2</sub>), centrifuged (6000 rpm for 10 min) and resuspended in PBS. The resulting nuclear suspension was counted by hemocytometer and held on ice until analysis. Microscopic examination revealed a suspension of individual nuclei with  $<5\%$  intact cells. Counts of the original cell suspension and the final nuclear suspension showed that this procedure resulted in a 50%–60% recovery of nuclei. Counts performed after light scatter analysis showed that there was no further loss of nuclei even after several hours of storage in PBS on ice.

### 2.4 Cell Cycle Analysis

An aliquot containing  $10^6$  cells was pelleted by centrifugation ( $1000 \times g$ , 10 min), resuspended in PBS, and fixed in 70% ethanol. Fixed cell samples were washed once with PBS and then resuspended in PBS containing 50  $\mu\text{g}/\text{mL}$  propidium iodide (Sigma) with 100  $\mu\text{g}/\text{mL}$  RNase Type I (Sigma Chemicals). Stained samples were analyzed on a flow cytometer (Becton Dickinson FACS Calibur) to collect DNA content histograms containing  $>10^4$  cells. Histograms were analyzed for cell cycle phase distribution with MacCycle (Phoenix Flow Systems) using correction for background debris and aggregates.

### 2.5 Measurement of Nuclear Size and Shape

Suspensions of nuclei and cells were spun onto glass slides (Cytospin) and air dried. A solution of 10  $\mu\text{g}/\text{mL}$  Hoechst 33342, a DNA-specific fluorochrome, in phosphate-buffered saline was dropped onto the cell spot and covered with a glass coverslip. Images of nuclei were obtained using a fluorescent microscope (Zeiss) at 20X magnification and digitized using a cooled charge coupled device camera. Digital images were analyzed using the NIH Image software package to determine major and minor axes for each of 100 nuclei. Geometric mean diameters and the ratio of major:minor axes (ellipticity) were calculated for each nucleus. Nuclei size distributions were calibrated by measuring 100 fluorescent microspheres (Coulter) 10  $\mu\text{m}$  in diameter. Comparison with the manufacturer's specifications for the spheres indicated an image measurement accuracy of 2%–3%. Measurements of nuclei in in-

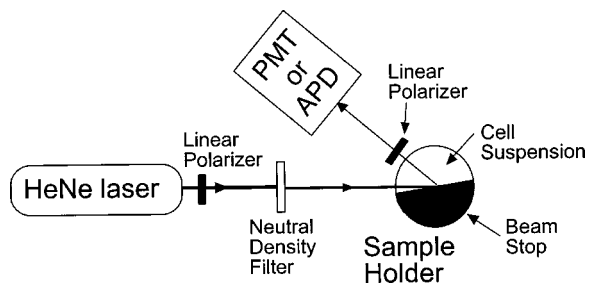


**Fig. 1** A schematic of the polarized angular dependent scattering system. A 633 nm light is incident through a linear polarizer onto a dilute suspension of biological cells or isolated nuclei. Scattered light is collected through a second linear polarizer and detected with either a photomultiplier tube (PMT) or an avalanche photodiode.

tact cells compared to nuclear suspensions prepared from the same cell sample showed no significant difference in diameter or ellipticity. Comparison of air-dried samples to measurements on fresh nuclei showed no significant effect of cytospinning and drying.

## 2.6 Angular Dependent Scattering Measurements

Angular dependent light scattering measurements were made using different combinations of linear polarizers (Versalight, Meadowlark Optics) for light delivery and detection. A schematic of the measurement system is shown in Figure 1. The polarizers were chosen because of their high throughput, 96% of the light of the chosen polarization is passed, and their high extinction ratio (2500:1). Three types of polarized angularly resolved light scattering measurements were performed. In one case both the polarizer in front of the laser and the polarizer in front of the detector were oriented so as to pass light polarized parallel to the scattering plane. In the second case, the polarizers were oriented so as to both pass light perpendicular to the scattering plane. Finally, measurements were made with one polarizer passing light polarized parallel to the scattering plane and the second polarizer passing light polarized perpendicular to the scattering plane. We found that for this third case the data did not depend on which polarizer was oriented in which direction. We also made measurements without any polarizers in the beam as a self-consistency check.

About half of the angular dependent measurements of scattering from cells were made with a photomultiplier tube (PMT) as the light detector. The disadvantage of the PMT (Hamamatsu R928) as a detector is its limited dynamic range. Consequently, optical density filters had to be inserted into the beam to reduce the incident light intensity when forward scattering was being measured. The other half of the measurements on epithelial cells and all of the measurements of isolated nuclei were made with an avalanche photodiode as a detector (Hamamatsu C5460-01 APD module). With this change most measurements were made without an optical density (OD) filter in the beam path—only at angles less than about 30° was a 1 OD filter needed.

Two different sample cells were used for the angular dependent light scattering measurements. The one shown in Figure 1 has a beam stop so that back reflection off of the sample cell does not swamp the light scattered at high angles from the

biological samples. A sample cell without a beam stop was used for measuring scattering at angles less than about 30°. Both sample cells were placed on a stage cooled to about 7 °C. The concentration of epithelial cells varied from 100 000 to 500 000/mL. Previously, we have found that at concentrations up to 200 000 fibroblast cells/mL multiple scattering is insignificant.<sup>19,20</sup> When multiple scattering becomes a problem, it first shows up at the smallest and largest angles as an apparent loss in angular resolution. With these epithelial cells we did not see any significant (i.e., larger than other sources of error) change in results when the concentration was varied from 100 000 to 500 000/mL. The concentration of isolated nuclei was 700 000/mL. Because the isolated nuclei scatter roughly half as strongly as the whole cells, there was still no problem with multiple scattering. The angular resolution of the system is 1.3°. From 6° to 20°, measurements were made in 2° or 3° increments. Measurements were made in 5° increments from 20° to 170° with the exception of measurements from 85° to 100° made with the polarizers passing light oscillating parallel to the scattering plane which were made in 1° or 2° increments.

## 2.7 Data Manipulation

Some of the measurements with both polarizers passing light polarized perpendicular to the scattering plane were multiplied by a factor such that, the probability of scattering through an angle  $\theta$ ,  $P(\theta)$ , integrates to 1 as in Eq. (1). For each sample, the three types of polarized light scattering measurements were multiplied by the same factor. The purpose of this procedure was to enable comparison of the angular dependence of the light scattering without concern for the exact concentration of cells which were measured

$$\int P(\theta) \sin \theta d\theta = 1. \quad (1)$$

## 2.8 Calculations of Light Scattering

To calculate light scattering from spheres we used a modified version of the code of Bohren and Huffman.<sup>21</sup> The modifications allowed us to calculate the angular dependent scattering from Gaussian and log-normal distributions of particle sizes rather than just a monodisperse distribution. The user provides the mean radius and the width of the distribution. The distribution is discretized with a radius step size of the standard deviation divided by 10.0 unless this step size is greater than the mean radius divided by 5.0, in which case the step size is the mean radius divided by 10.0. The wings of the distribution are cut off at a value of 1% of the peak value when two log-normal distributions are used and at a factor of  $10^{-8}$  of the peak value when a single log-normal distribution was used. To calculate scattering from ellipsoidal particles we used the T-matrix code of Mishchenko and Travis<sup>22</sup> which can be found at [http://www.giss.nasa.gov/~crmim/t\\_matrix.html](http://www.giss.nasa.gov/~crmim/t_matrix.html).

## 2.9 Data Fitting and Minimization Routines

As described in the analysis section, the cells and isolated nuclei were modeled as consisting of many small particles, and calculations using this model were fitted to the experimental results. The minimization routine used was the down-

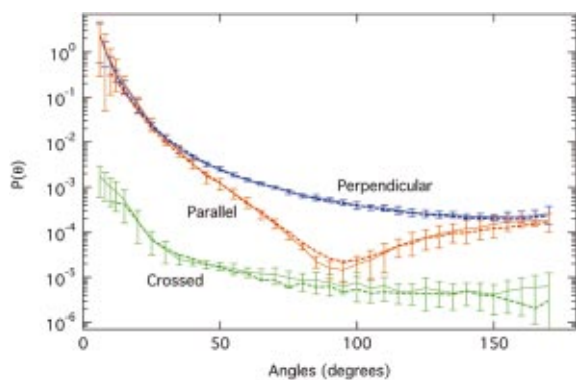


**Fig. 2** The results of angular dependent light scattering measurements of AT3.1 and AT6.1 cells. Solid lines: AT3.1 cells. Dashed lines: AT6.1 cells. Polarization perpendicular to the scattering plane: blue. Polarization parallel to the scattering plane: red. Polarizers crossed: green. All curves are the average of three or more measurements of separate cell preparations. Standard deviations are shown for the AT3.1 cells and are very similar for the AT6.1 cells.

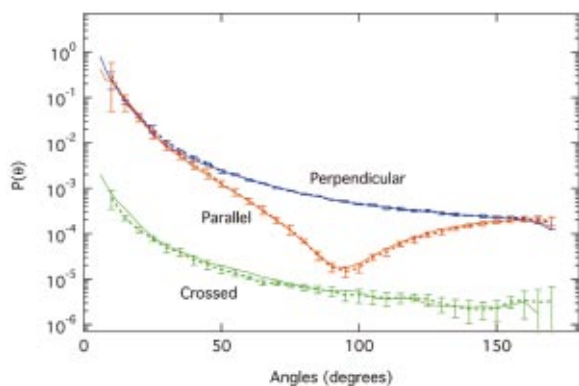


**Fig. 3** The results of angular dependent light scattering measurements of nuclei isolated from AT3.1 cells and of nuclei isolated from AT6.1 cells. These results are averages for three preparations of nuclei from each type of cell. Standard deviations are shown for the nuclei isolated from AT6.1 cells and are very similar for the nuclei isolated from the AT3.1 cells. The color scheme is as described in Figure 2.

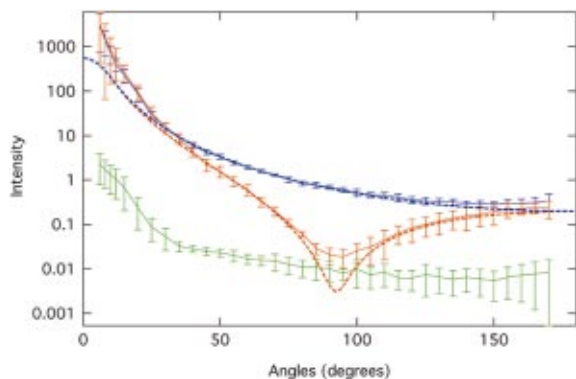


**Fig. 4** Comparison of a model fit using a single log-normal distribution of spheres (dashed lines) to experimental scattering data of AT3.1 cells (solid lines). Blue: polarization parallel to the scattering plane. Red: polarization perpendicular to the scattering plane. Green: polarizers crossed. The fit value for crossed polarizers is 0 and not shown on the log scale.

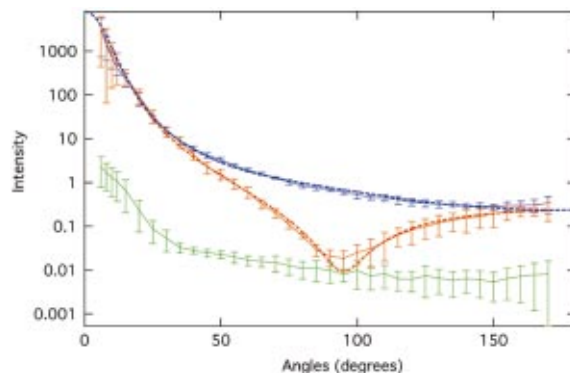


**Fig. 5** Comparison of a model fit using two log-normal distributions of spheres to experimental scattering data of AT3.1 cells. The curves are as described in Figure 4.

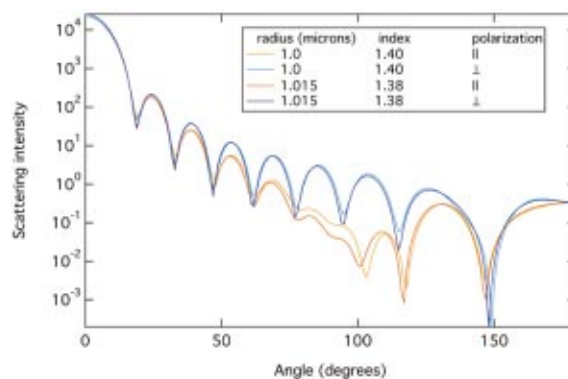


**Fig. 7** Scattering from spheres of radius 1.000  $\mu\text{m}$  with an index of 1.40 (light colors: orange and light blue) compared to scattering of spheres with a radius of 1.015  $\mu\text{m}$  with an index of 1.38 (dark colors: red and blue). The orange and red results are for scattering light polarized perpendicular to the scattering plane. The blue results are for scattering of light polarized parallel to the scattering plane.

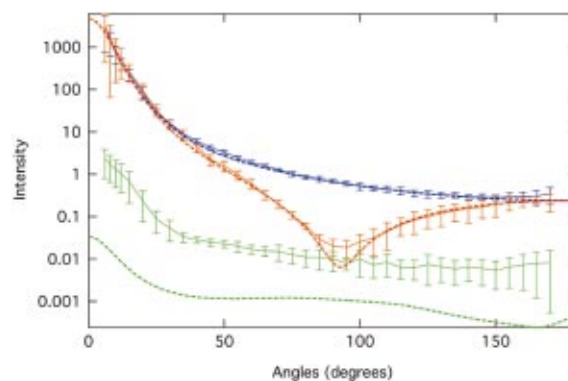


**Fig. 8** Comparison of a model fit using two log-normal distributions of ellipsoids to experimental scattering data of AT3.1 cells. The curves are as described in Figure 4.

hill simplex method as implemented in Ref. 23. The data were fitted over the angle range 15–160° using chi squared as the fit criteria. We noticed that the results depended weakly on the starting parameters for the fits, suggesting that the fitting surface either had a very shallow minima or multiple minima. All data were fit multiple times with different starting conditions and the fit resulting in the smallest chi squared is presented. The error in the fits was estimated by looking at the difference in fit coefficients for the average measurements versus fits to individual measurements.

### 3 Results

#### 3.1 Experimental Results

Figure 2 shows the results of angular dependent light scattering measurements of AT3.1 cells and AT6.1 cells. The data for the AT3.1 and AT6.1 epithelial cells are very similar. Figure 3 shows the light scattering results for isolated nuclei from AT3.1 and AT6.1 cells, respectively. The angular dependent light scattering from the nuclei is quite similar to the scattering from whole cells, although there is slightly less forward scattering from the nuclei.

The cells were counted before and after the light scattering measurements. In all cases the fraction of particles in the suspension before the measurements which were whole cells was greater than 95%. We found that on average there was a very small amount of degradation of the cells during the light scattering measurements and the ratio of debris (i.e., fragments of cells) to cells increased by 1%–2%.

Cell cycle analyses demonstrated that the percent of cells in the G1 phase of the cell cycle varied from 34% to 60% for the AT3.1 cells and from 32% to 59% for the AT6.1 cells. Therefore, all the cell cultures were still reproducing at time of harvest and none had reached the plateau phase of growth.

Image analysis was used to determine the size of nuclei isolated from AT3.1 and AT6.1 cells. The histograms of nuclear diameter were fit to log-normal distributions [Eq. (2)]. For the AT3.1 nuclei we obtained a mean of 8.3  $\mu\text{m}$  and  $\sigma = 0.11 \mu\text{m}$ . For the AT6.1 nuclei, the mean was 9.9  $\mu\text{m}$  and  $\sigma = 0.15 \mu\text{m}$ . We found that the nuclei were not perfectly spherical. The average ratio of the two axes from image analysis was 1.2 for both the AT3.1 and AT6.1 nuclei.

#### 3.2 Analysis and Computational Results

In order to have a tractable modeling problem it is sometimes assumed that some or all of the scattering structures in epithelial cells are spherical, noninteracting, and have a single refractive index relative to the medium. We initially analyzed our data based on these assumptions. We then evaluated the effects of these assumptions and removed some of them. Figure 4 shows the results of fitting our light scattering data for AT3.1 cells to a model with one log-normal distribution [Eq. (2)] of sphere sizes

$$F(r) = 1/r^* \exp[-(\ln(r) - \ln(r_m))^2 / 2\sigma^2]. \quad (2)$$

In Eq. (2),  $r_m$  is the mean of the distribution and  $\sigma$  is a parameter determining the width of the distribution. For the fit shown in Figure 4, the refractive index of the medium was set at 1.332, the value for water. This value was chosen because

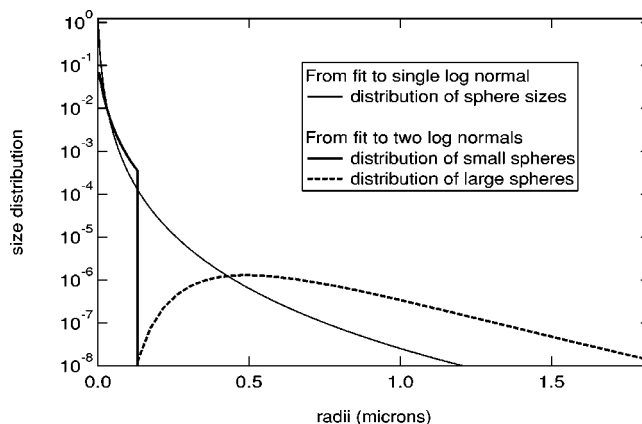


**Fig. 6** The scatterer size distributions used to obtain the fits shown in Figures 4 and 5. The thin black curve is the size distribution for the fit in Figure 4. The two thick black curves are the two log-normal distributions used to obtain the fit shown in Figure 5.

we hypothesize that much of the scattering is from organelles and structures in the cytoplasm—the appropriate index to use is then the index of cytoplasm when the scattering structures have been removed. When the organelles and possibly light scattering molecules such as protein and DNA are removed, the index of the “cytoplasm” should be very close to that of water. The scatterer index was held at 1.39, a value within the range of refractive indices of structures within cells.<sup>24</sup> The result of Figure 4 is that chi squared was minimized with  $r_m = 0.00312 \mu\text{m}$  and  $\sigma = 1.22 \mu\text{m}$ . This model results in a fairly poor fit to the data. Because the scatterers are spherical, no light is scattered with a polarization crossed relative to the incident polarization. Consequently, in the model fit the cross-polarized intensity is zero and is not shown in the log plot of Figure 4. Furthermore, scattering at small angles is underestimated, and the scattering with light polarized parallel to the scattering plane is underestimated at 90°. To address these issues, we increased the complexity of our model and used two log-normal distributions. An example of the results obtained by fitting the light scatter results for AT3.1 cells with a size distribution of particles consisting of two log normals is shown in Figure 5. As with the fit to a single log-normal distribution, the index of the spheres was held at 1.39 while the index of the medium was 1.332. The size distributions giving the fits shown in Figures 4 and 5 are plotted in Figure 6. There appear to be a large number of particles with radii on the order of 10’s–100’s of nanometers in radius that scatter light. There is also evidence for light scattering off of particles the size of mitochondria, lysosomes, and peroxisomes.

To examine the effect of changing the refractive index we performed Mie scattering calculations with a medium index of 1.33 and with sphere indices varying from 1.35 to 1.42. For spheres of 50 nm or less in radius there is no change in the shape of the angular dependent scattering curves when the polarization is parallel or perpendicular to the scattering plane. In the language of Mueller matrices this is the same as saying that the angle dependencies of matrix elements  $S_{11}(\theta)$  and  $S_{12}(\theta)$  do not depend on refractive index. There is, however, a factor of 20 increase in the scattering coefficient as the index increases from 1.35 to 1.42. For larger particles there is a change in the shape of  $[S_{11}(\theta) - S_{12}(\theta)]$  and  $[S_{11}(\theta) + S_{12}(\theta)]$  as the index of the spheres is increased. To a large

**Table 1** Particle size distribution parameters obtained by fitting experimental light scattering data to model calculations of scattering from spheres. The results in columns labeled cells and nuclei describe the size of the particles believed to be responsible for light scattering from cells and nuclei, respectively. The error in the mean radius of the smaller size distribution is  $0.0015 \mu\text{m}$ . The error in  $\sigma$  for smaller distribution is  $0.2 \mu\text{m}$ . The error in the mean size of the larger distribution is  $0.2 \mu\text{m}$  and the error in  $\sigma$  for the larger distributions is  $0.15 \mu\text{m}$ . The "ratio" is the factor by which the light scattering from the distribution of larger particles was multiplied. The error in this value is about 50% of the given number.

	AT3.1 cells	AT3.1 nuclei	AT6.1 cells	AT6.1 nuclei
Index=1.39				
Radius 1	$0.012 \mu\text{m}$	$0.011 \mu\text{m}$	$0.009 \mu\text{m}$	$0.012 \mu\text{m}$
$\sigma$ 1	$1.15 \mu\text{m}$	$1.15 \mu\text{m}$	$1.14 \mu\text{m}$	$1.04 \mu\text{m}$
Radius 2	$0.59 \mu\text{m}$	$0.55 \mu\text{m}$	$0.60 \mu\text{m}$	$0.65 \mu\text{m}$
$\sigma$ 2	$0.43 \mu\text{m}$	$0.73 \mu\text{m}$	$0.55 \mu\text{m}$	$0.67 \mu\text{m}$
Ratio	0.000 64	0.000 21	0.000 21	0.000 04
Index=1.37				
Radius 1	$0.012 \mu\text{m}$	$0.011 \mu\text{m}$	$0.013 \mu\text{m}$	$0.011 \mu\text{m}$
$\sigma$ 1	$1.05 \mu\text{m}$	$1.20 \mu\text{m}$	$1.01 \mu\text{m}$	$1.23 \mu\text{m}$
Radius 2	$0.58 \mu\text{m}$	$0.52 \mu\text{m}$	$0.57 \mu\text{m}$	$0.51 \mu\text{m}$
$\sigma$ 2	$0.69 \mu\text{m}$	$0.77 \mu\text{m}$	$0.90 \mu\text{m}$	$0.80 \mu\text{m}$
Ratio	0.000 35	0.000 17	0.000 29	0.000 15

extent, this change in index can be compensated for by a small change in the size of the sphere. In Figure 7 light scattering from a sphere of radius  $1.0 \mu\text{m}$  and index 1.40 is very similar to the scattering from a sphere of radius  $1.015 \mu\text{m}$  and an index of 1.38. In conclusion, the effects of modeling the spheres as all having the same index of refraction when, in fact, they have different indices, is a small distortion in the size distribution obtained. For example, if the index used was higher than the actual index of the small spheres (i.e., 50 nm and less in radius), the estimate of the number density of small spheres will be low. For large spheres (i.e., on the order of a few microns in radius) a high estimate of the index of refraction results in an underestimation of scatterer size.

To further investigate the effects of changing the refractive index, we fitted the experimental data using two different values of the scatterer refractive index, 1.37 and 1.39, while keeping the medium index at 1.332. The fitting parameter results are given in Table 1. We had expected that the results for the size distribution with an index of 1.37 would be similar to those with an index of 1.39, except that the size distribution is slightly distorted and slightly larger. However, in most cases the use of a different refractive index resulted in a model fit with slightly different scattering characteristics, i.e., the shape of the scattering curves changed slightly. Because we are not able to precisely fit the experimental data, changes in how the data are fit swamp the expected changes in the scattering size distribution.

In reality the scatterers in cells are not spherical. Consequently, we implemented a model in which the scatterers were prolate ellipsoids. The ellipsoids were characterized by a radius of an equal volume sphere and the ratio of the ellipsoid axes. The ratio of large to small axes was limited to 2 for the distribution of larger scatterers (i.e., the distribution with a mean radius of about  $1 \mu\text{m}$ ) because of problems with convergence of the T-matrix code. For the distribution of smaller scatterers (i.e., the distribution with a mean radius of about  $0.01 \mu\text{m}$ ), the ratio of large to small axes was varied up to a factor of 10. The result of fitting AT3.1 cells to a model with two log-normal distributions of ellipsoids is shown in Figure 8. One of the log-normal distributions had a mean radius of  $0.013 \mu\text{m}$  and  $\gamma = 1.18 \mu\text{m}$ . The ratio of the axes of the ellipsoids in this distribution was 4:1. The second log-normal distribution had a mean radius of  $0.50 \mu\text{m}$  and  $\gamma = 0.48 \mu\text{m}$ . The ratio of the corresponding ellipsoid axes was 2. The amplitude ratio of the two distributions was 0.000 75. These results can be compared to those in Table 1 where the scatterers were assumed to be spherical. The amplitude ratio of the two distributions was quite similar. The mean of the distribution of smaller particles is nearly the same ( $0.013$  instead of  $0.012 \mu\text{m}$ ), however, the width is quite a bit larger. The mean of the second distribution is slightly smaller,  $0.50 \mu\text{m}$  compared to  $0.59 \mu\text{m}$  and the width is also slightly smaller. There are then two main effects on the resultant size distribution of changing from spheres to ellipsoids: the dip between the two distributions shifts from the value of  $0.13 \mu\text{m}$  seen in Figure 6 to a value of  $0.2 \mu\text{m}$  and the maximum radius is reduced from the value of  $1.83$  to  $0.96 \mu\text{m}$ .

The light scattering contributions of the large (mean radius= $0.5 \mu\text{m}$ ) and small (mean radius= $0.013 \mu\text{m}$ ) ellipsoidal particle distributions are given in Figure 9. The larger particles are the primary scatterers of light at small angles. Scattering from smaller particles is responsible for the nearly constant scattering probability at angles greater than  $120^\circ$  for light polarized perpendicular to the scattering plane.

The effects of changing the refractive index of nonspherical scatterers are slightly different than the effects for spherical scatterers. Calculations of light scattering from prolate ellipsoids with a major/minor axes ratio of 10 and a sphere-equivalent radius of 50 nm are shown in Figure 10. The refractive index of the scatterers was varied while the refractive index of the medium was held at 1.33. Figure 10 demonstrates that changing the ellipsoid refractive index does not affect the angular dependence of light scattering when the polarization is either perpendicular or parallel to the plane. However, the index of refraction of the scatterer does have an affect on the light scattered with a crossed polarization. Both the angular dependence and the amplitude relative to the amount of light scattered with the polarizer parallel changes. Also, we found that the cross section for scattering increases as the relative index of the scatterers increases. Figure 11 demonstrates the effect of changing the refractive index of larger particles. Scattering from prolate ellipsoids with a major/minor axes ratio of 2 and a sphere-equivalent radius of  $1.000 \mu\text{m}$  is shown. The dip in the angular dependent scattering of light polarized parallel to the scattering plane shifts to higher angle as the index is increased. Concurrently, the amplitude of the light scattered cross polarized to the incident

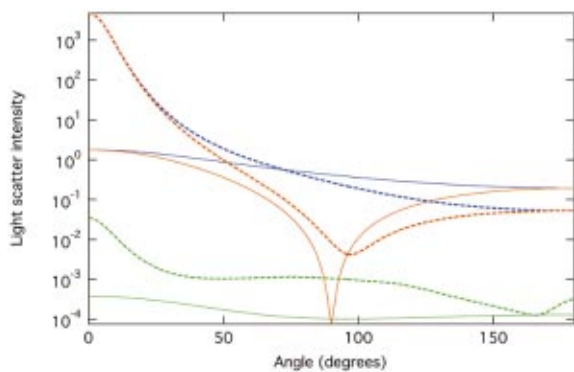


**Fig. 9** The scattering contribution from the small and large particle size distributions used in the fit in Figure 8. Dashed lines: contribution from the larger particle distribution. Solid lines: contribution from the smaller particle distribution.

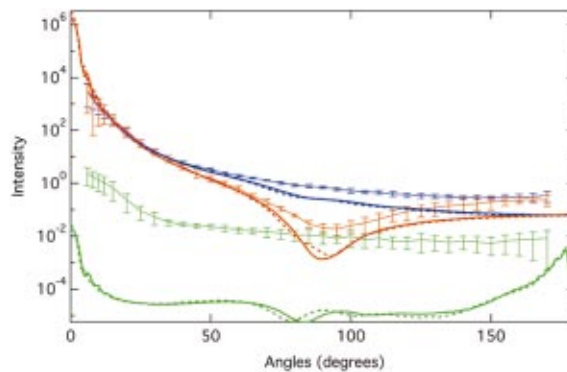


**Fig. 12** Comparison of experimental data to light scattering calculated from log-normal distributions of prolate spheroids representing nuclei. The color scheme is as described in Figure 4. The thick solid lines are calculated for a log-normal distribution with a mean radius of 4.13  $\mu\text{m}$  and  $s=0.65 \mu\text{m}$ . The thick dashed lines are calculated for a log-normal distribution with a mean radii of 4.95  $\mu\text{m}$  and  $\sigma=0.075 \mu\text{m}$ .

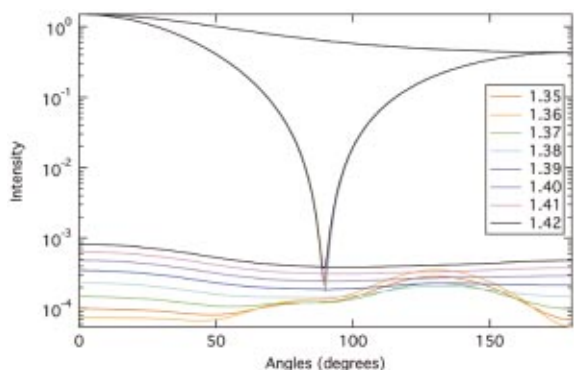


**Fig. 10** Calculations of light scattering for prolate ellipsoids with a sphere-equivalent radius of 50 nm. The ratio of major to minor axes was 10. The index of the ellipsoids was varied as shown in the caption. The index of the medium was 1.332. The results have been scaled to demonstrate that the shape of the scattering curves for light polarized either parallel or perpendicular to the scattering plane does not change with index. The results for light polarized perpendicular to the scattering plane are the top nearly straight set of curves. The results for light polarized parallel to the scattering plane show a sharp dip near 90°.

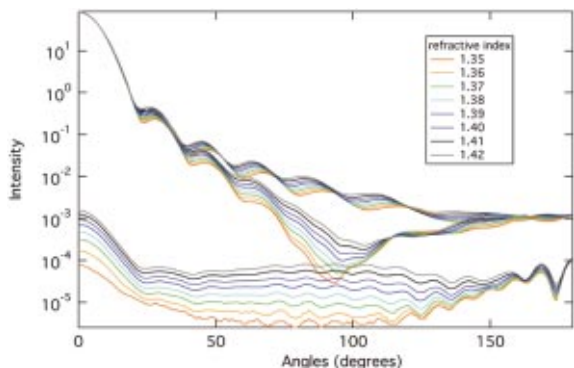
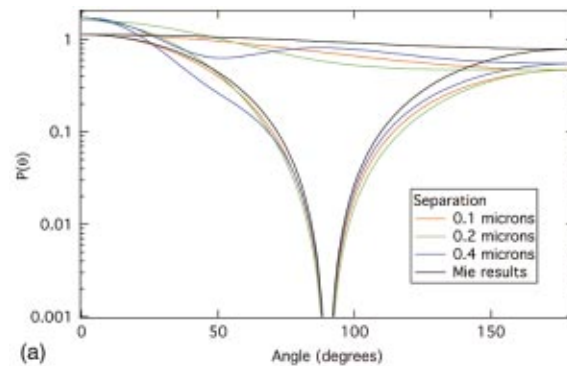
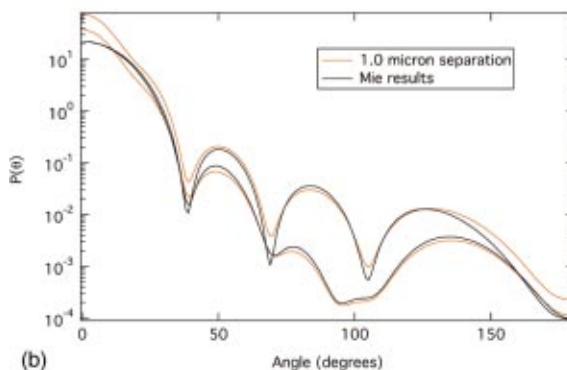


**Fig. 11** Scattering from prolate ellipsoids with a sphere-equivalent radius of 1.000  $\mu\text{m}$  as a function of scatterer refractive index. The ratio of major to minor axes was two. The index of the ellipsoids was varied as shown in the caption. The index of the medium was 1.332. The top set of curves is calculated light scattering when the polarizers transmit light polarized perpendicular to the scattering plane. The set of curves having a dip near 90 to 100° is calculated light scattering when the polarizers transmit light polarized parallel to the scattering plane. The bottom set of curves is for crossed polarizers.



(a)



(b)

**Fig. 13** (a) Calculations of scattering from pairs of 0.05  $\mu\text{m}$  spheres in close proximity to each other compared to the scattering from isolated spheres of 0.05  $\mu\text{m}$  in radius. (b) Calculation of scattering from a pair of 0.5  $\mu\text{m}$  radius spheres in close proximity compared to scattering from isolated 0.5  $\mu\text{m}$  radius spheres. In both cases the index of the medium was 1.33 and the index of the spheres was 1.4

light increases. Unlike the case of spherical scatterers, a larger scatterer will not compensate for a lower index of refraction. We increased scatterer size while holding the refractive index of the scatterers at 1.35 and the medium index at 1.33. The dip at  $90^\circ$  did not shift to higher angles and the amplitude of cross polarized scattering did not increase. We did, however, see an increase in the relative amount of forward scattering (data not shown). Consequently, the scatterer index is a truly independent parameter in the case of ellipsoids in contrast to spheres.

There have been several reports in the literature that nuclear size can be determined from light scattering measurements if the nuclei are assumed to be homogeneous.<sup>8,25</sup> Therefore, we tested a hypothesis that our angular dependent light scattering data could be explained by scattering from homogeneous particles the size of nuclei. Angular dependent scattering was calculated from distributions of prolate spheroids. The size distribution and ratio of major and minor axes used were those obtained by image analysis of the nuclei. The nuclei were assumed to have an index of 1.39 and the cytoplasm an index of 1.37 for the calculation in accordance with one of the literature reports of the refractive index of the nucleus and cytoplasm.<sup>26</sup> These values resulted in a relative refractive index of 1.015. There are significant differences between the calculation and the experimental results as seen in Figure 12. The calculations showed significantly less scattering at the large angles than the experimental results. This difference increases if a larger relative refractive index is used as is sometimes done. A further discrepancy between these calculation results and the experimental results is that the cross-polarized intensity is two orders of magnitude too low.

Finally, we considered the fact that cells are not made up of individual scatterers; rather they are composed of structures of many shapes sometimes within an optical wavelength of each other. To investigate how the close proximity of scatterers might affect how they scatter light we used the bisphere scattering code of Mishchenko and collaborators.<sup>27,28</sup> The effects of proximity of the scattering from two spheres of radii  $0.05 \mu\text{m}$  are shown in Figure 13(a). Compared to the Mie scattering results for dispersed spheres, there is relatively more scattering at small angles and less at the large angles when the spheres are in close proximity. There is also a 50% increase in the scattering coefficient,  $\mu_s$ . Figure 13(b) shows the effects of scatterers being in close proximity for spheres of radius  $0.5 \mu\text{m}$ . When the spheres are touching there is a very slight increase in the amount of light scattered in the forward and backward directions and a 15% increase in  $\mu_s$ . At larger separations, this effect is greatly diminished. Based on these results, we can provide qualitative estimates of the affect of scatterers being in close proximity. If particles on the order of 50 nm in size are in close proximity rather than dispersed, the actual distribution of particle sizes will contain 33% less of these size particles than our calculations estimate. Second, the size of these particles will be slightly smaller than was estimated assuming the particles were dispersed. If particles on the order of  $0.5 \mu\text{m}$  are in close proximity rather than dispersed, then the actual particle size distribution would contain about 13% less particles of that size.

#### 4 Discussion

We were able to describe polarized, angular dependent light scattering data from cells or isolated nuclei as scattering from

broad size distributions of scatterers. A wide variety of scatterer sizes is needed in order to describe the experimental data and the number of small (i.e.,  $\sim 10^3$  of nm) structures scattering light exceeds the number of large ( $\sim 1 \mu\text{m}$ ) structures scattering light by  $10^4$  as shown in Figure 6. The largest scatterer was  $\sim 2 \mu\text{m}$  in radius when the scatterers were assumed to be spheres and  $\sim 1 \mu\text{m}$  in radius when the scatterers were assumed to be ellipsoids. This size is smaller than a nucleus which is about  $4.5 \mu\text{m}$  in radius and much smaller than the cell radius which is about  $7 \mu\text{m}$ . This result is somewhat surprising since both structures are expected to contribute to light scattering. Possibly, it was not necessary to incorporate scatterers the size of cells into our model because we did not measure light scattering at angles less than  $10^\circ$ . Cell size can be determined by light scattering measurements in the angle range  $0.5\text{--}1.5^\circ$ .<sup>29</sup>

The fact that there are no scatterers the size of nuclei in our size distribution is somewhat surprising in light of reports in the literature that angular dependent light scattering is sensitive to nuclear size. Experimental observations of scattering at angles less than about  $25^\circ$  have been attributed to scattering from the nuclei. Measurements of Chinese hamster ovary cells showed a fine structure between  $2.5$  and  $25^\circ$  which could be modeled as a coated sphere, i.e., a nucleus surrounded by cytoplasm.<sup>26</sup> This fine structure has not been seen in other cell types either by others or by the same authors.<sup>26</sup> Other evidence that angular dependent light scattering is sensitive to nuclear size comes from finite-difference time domain (FDTD) simulations of scattering from cells. These computations show that scattering in the angle range less than  $20^\circ$  is sensitive to nuclear size.<sup>24</sup> In particular, scattering at angles less than  $10^\circ$  increases as nuclear size increases.

Clearly, scattering from homogeneous nuclei alone cannot account for our experimental results as demonstrated by Figure 12. However, some of the scattering from cells could be from particles the size of the nucleus. For the fit shown in Figure 8, the relative refractive index was 1.044. If a smaller relative refractive index was used, then larger particles might have been incorporated into the fit since for spheres and only slightly nonspherical ellipsoids a change in size can approximately compensate for a change in index. Even with this change, however, nuclei would be only a minor contributor, because significant scattering from smaller particles, with higher indices and more ellipticity, is needed in order to generate enough backscattering to reproduce the experimental data, and to have cross-polarized intensity. In the future better quantification of the contribution of particles the size of nuclei to angular dependent light scattering could be obtained by measurements at smaller angles and using more complicated models with varying refractive indices.

The data shown in Figure 6 and the data in Table 1 indicate that there are scatterers as small as a few angstroms in size in cells. It is important to note that our measurements of light scattering are insensitive to whether a particle is 10 nm in size or smaller. Therefore, the shape of the scattering distribution below 10 nm is controlled only by the number of particles needed with a size of 10 nm or less and by the shape of the distribution needed for larger particles.

When obtaining quantitative information about nuclear size from light scattering measurements it is frequently assumed that the nuclei are homogeneous. The results presented

here indicate that the nuclei are quite inhomogeneous. In fact, we did not find significant differences between the angular dependent light scattering properties of isolated nuclei and of whole cells aside from a small difference in the relative amount of forward scattering which has been previously reported.<sup>19,20</sup> At large angles, the angular dependence of light scattering appears to be very similar for cells and isolated nuclei and can be modeled with nearly the same distribution of structure sizes. It is, therefore, likely that backscattering measurements such as those typically implemented in *in vivo* situations may be sensitive to changes in the scattering from nuclear structures such as macromolecules and nucleoli. Recent FDTD model calculations have shown that hypothetical internal index of refraction variations in nuclei can greatly increase backscattering.<sup>30</sup> Additionally, backscattering of both cells and nuclei has been shown to correlate with increased DNA content.<sup>20</sup> Future work will be needed to confirm whether light scattering is sensitive to changes such as those represented by hyperchromaticity in neoplastic cells or nucleoli number.

There are some significant discrepancies between our model fits and the experimental data as shown in Figures 5 and 8. The dip at 90° in the scattering of light polarized parallel to the table is deeper for the model than for the measurements, although for the case of spherical scatterers, the fit is within the errors of the experimental data. The second major difference is that the amount of light scattered cross polarized is much greater in the experimental data than for the model. The low values obtained for light scattered with a polarization perpendicular to the incident light polarization may be due to the fact that we were unable to use ellipsoids with major to minor axes ratios greater than two for the larger (~1 μm) distribution of particles. Additionally, the assumption that scatterers are ellipsoidal in shape may not be close enough to the shape of the scattering structures. Structures of a different shape might give more scattering of a crossed polarization. A further possibility is that the index of refraction of the scattering particles is greater than 1.39. As demonstrated in Figure 10, increasing the index of refraction of the scattering centers can increase the amount of cross-polarized scattering.

We have investigated how the estimation of structure size depends on whether the scatterers are considered to be ellipsoidal or spherical in shape, on the exact value of the refractive index chosen for the scatterers, and on the proximity of the scatterers. The sizes of the scattering particles did not change significantly when the shape of the scattering centers was changed from spheres to ellipsoids as can be seen by comparing the results for fitting the light scattering data for AT3.1 cells with a distribution of ellipsoids to the results in Table 1. Even for the distribution with a ratio of ellipsoid axes of 4, there is no significant change in the mean and width of the size distribution. Concerning the effects of refractive index changes, we found that when the refractive index of the scatterers was changed from 1.37 to 1.39, the sizes of the scattering centers were nearly unchanged, as can be seen in Table 1. However, the range of relative refractive indices we tested from  $1.37/1.332=1.0285$  to  $1.39/1.332=1.044$ , may not cover the full range found in tissue. The cytoplasm of cells is estimated to have an average refractive index of 1.37 as measured by index matching techniques.<sup>9</sup> The refractive index of nuclei has been measured to be 1.39 which gives a

relative index of 1.015. Extrapolating from the results in Figure 7, a change in relative index from 1.028 to 1.015 would increase scatterer size by ~1.5%. On the other hand, the refractive index of proteins has been estimated to be 1.50.<sup>31</sup> If these proteins are free in the cytoplasm (i.e., surrounded by water), then the relative index is  $1.50/1.33=1.128$ . An increase in the relative index from 1.044 to 1.128 could decrease the estimate of the number particles the size of proteins by a factor of 30. Finally, considering the proximity of scattering particles, we did not find large changes in the scattering properties of particles in close proximity.

A future question to be addressed is how refractive index structures of different sizes contribute to light scattering signals that can be measured *in vivo*. For example, what structures control the amount of light that returns to the detector? The work presented in this paper facilitates the computations needed to answer that question by providing a quantitative description of the size and shape of scattering centers in epithelial cells. Based on the calculable scattering properties of the various scattering centers and their relative concentrations, Monte Carlo simulations can be used to determine whether the many small particles with their small cross section and isotropic scattering are primarily responsible for light being reemitted on the same surface for which it was incident or whether the larger particles with their large cross section and highly forward directed scattering turn the light around. Potentially, light scattering may be sensitive to structural features that are not commonly measured by pathologists and may provide medical information not previously available.

## Acknowledgments

We gratefully acknowledge the assistance of Thomas Yoshida and Dr. Babetta Marrone for training on and use of the Zeiss fluorescent imaging system. We also acknowledge Vijaya Doddi for technical assistance with cell culture and cell cycle analysis. This work was supported by NIH Grant Nos. CA71898, CA89255, and CA51150.

## References

1. B. F. Hochheimer, "Polarized light retinal photography of a monkey eye," *Vision Res.* **18**, 19–23 (1978).
2. S. R. Pal and A. I. Carswell, "Polarization anisotropy in lidar multiple scattering from atmospheric clouds," *Appl. Opt.* **24**, 3464–3471 (1985).
3. M. Dogairu and T. Asakuru, "Polarization-dependent backscattering patterns from weakly scattering media," *J. Opt. (Paris)* **24**, 271–278 (1993).
4. A. H. Hielscher, J. R. Mourant, and I. J. Bigio, "Influence of particle size and concentration on the diffuse backscattering of polarized light from tissue phantoms and biological cell suspensions," *Appl. Opt.* **36**, 125–135 (1997).
5. B. D. Cameron, M. J. Rakovic, M. Mehrubeglu, G. W. Kattawar, S. Rastegar, L. V. Wang, and G. L. Cote, "Measurement and calculation of the two-dimensional backscattering Mueller matrix of a turbid media," *Opt. Lett.* **23**, 485–487 and 1630 (1998).
6. A. H. Hielscher and S. Bartels, "Monte Carlo simulations of the diffuse backscattering Mueller matrix for highly scattering media," *Appl. Opt.* **39**, 1580–1588 (2000).
7. T. M. Johnson and J. R. Mourant, "Polarized wavelength-dependent measurement of turbid media," *Opt. Express* **4**, 200–216 (1999).
8. V. Backman, R. Gurjar, K. Badizadegan, I. Itzkan, R. R. Dasari, L. T. Perelman, and M. S. Feld, "Polarized light scattering spectroscopy for quantitative measurement of epithelial cellular structures *in situ*," *IEEE J. Quantum Electron.* **5**, 1019–1026 (1999).
9. K. Sokolov, R. Drezek, K. Gossagee, and R. Richards-Kortum, "Re-

- flectance spectroscopy with polarized light: Is it sensitive to cellular and nuclear morphology," *Opt. Express* **5**, 302–317 (1999).
10. J. R. Mourant, T. M. Johnson, and J. P. Freyer, "Characterizing mammalian cells and cell phantoms by polarized back-scattering fiber-optic measurements," *Appl. Opt.* (in press).
  11. S. L. Jacques, J. R. Roman, and K. Lee, "Imaging superficial tissues with polarized light," *Lasers Surg. Med.* **26**, 119–129 (2000).
  12. D. Bicout, C. Brosseau, A. S. Martinez, and J. M. Schmitt, "Depolarization of multiply scattered waves by spherical diffusers: influence of the size parameter," *Phys. Rev. E* **49**, 1767–1770 (1994).
  13. G. Jarry, E. Steimer, V. Damaschini, M. Epifanie, M. Jurczak, and R. Kaiser, "Coherence and polarization of light propagating through scattering media and biological tissues," *Appl. Opt.* **37**, 7357–7367 (1998).
  14. L. C. Junqueira, J. Carneiro, and R. O. Kelley, *Basic Histology*, Appleton and Lange, Norwalk, CT (1992).
  15. L. Stryer, *Biochemistry*, 3rd. ed., p. 760, Freeman, San Francisco (1988).
  16. J. M. Schmitt and G. Kumar, "Turbulent nature of refractive-index variations in biological tissue," *Opt. Lett.* **21**, 1310–1312 (1996).
  17. J. M. Schmitt and G. Kumar, "Optical scattering properties of soft tissue: a discrete particle model," *Appl. Opt.* **37**, 2788–2796 (1998).
  18. T. R. Tennant, H. Kim, M. Sokoloff, and C. W. Rinker-Schaeffer, "The Dunning model," *Prostate* **43**, 295–302 (2000).
  19. J. R. Mourant, J. P. Freyer, A. H. Hielscher, A. A. Eick, D. Shen, and T. M. Johnson, "Mechanisms of light scattering from biological cells relevant to noninvasive optical-tissue diagnostics," *Appl. Opt.* **37**, 3586–3593 (1998).
  20. J. R. Mourant, M. Canpolat, C. Brocker, O. Esponda-Ramos, T. Johnson, A. Matanock, K. Stetter, and J. P. Freyer, "Light scattering from cells: the contribution of the nucleus and the effects of proliferative status," *J. Biomed. Opt.* **5**, 131–137 (2000).
  21. C. F. Bohren and D. R. Huffman, *Absorption and Scattering of Light by Small Particles*, Wiley, New York (1983).
  22. M. I. Mischenko and L. D. Travis, "Capabilities and limitations of a current fortran implementation of the T-matrix method for randomly-oriented, rotationally symmetric scatterers," *J. Quant. Spectrosc. Radiat. Transf.* **60**, 309–324 (1998).
  23. W. H. Press, S. A. Teukolsky, W. T. Vetterling, and B. P. Flannery, *Numerical Recipes in C, The Art of Scientific Computing*, 2nd ed., Cambridge University Press, Cambridge (1992).
  24. R. Drezek, A. Dunn, and R. Richards-Kortum, "Light scattering from cells: finite-difference time-domain simulations and goniometric measurements," *Appl. Opt.* **38**, 3651–3661 (1999).
  25. L. T. Perelman, V. Backman, M. Wallace, G. Zonios, R. Manoharan, A. Nusrat, S. Shields, M. Seiler, C. Lima, T. Hamano, I. Itzkan, J. Van Dam, J. M. Crawford, and M. S. Feld, "Observation of periodic fine structure in reflectance from biological tissue: a new technique for measuring nuclear size distribution," *Phys. Rev. Lett.* **80**, 627–630 (1998).
  26. A. Brunsting and P. F. Mullaney, "Differential light scattering from spherical mammalian cells," *Biophys. J.* **14**, 439–453 (1974).
  27. M. I. Mischenko and D. W. Mackowski, "Electromagnetic scattering by randomly oriented bispheres: comparison of theory and experiment and benchmark calculations," *J. Quant. Spectrosc. Radiat. Transf.* **55**, 683–699 (1996).
  28. M. I. Mischenko, D. W. Mackowski, and L. D. Travis, "Scattering of light by bispheres with touching and separated components," *Appl. Opt.* **34**, 4589–4601 (1995).
  29. J. V. Watson, *Introduction to Flow Cytometry*, Chap. 10, Cambridge University Press, Cambridge (1991).
  30. R. Drezek, A. Dunn, and R. Richards Kortum, "A pulsed finite-difference time-domain (FDTD) method for calculating light scattering from biological cells over broad wavelength ranges," *Opt. Express* **6**, 147–157 (2000).
  31. K. F. A. Ros, *Phase Contrast and Interference Microscopy for Cell Biologists*, Chap. 7, p. 166, Arnold, London (1967).